

CFD Investigation of the effects of bubble aerator layouts on hydrodynamics of an activated sludge channel reactor

Rainier Hreiz, Olivier Potier, Jim Wicks & Jean-Marc Commenge

To cite this article: Rainier Hreiz, Olivier Potier, Jim Wicks & Jean-Marc Commenge (2018): CFD Investigation of the effects of bubble aerator layouts on hydrodynamics of an activated sludge channel reactor, Environmental Technology, DOI: [10.1080/09593330.2018.1448001](https://doi.org/10.1080/09593330.2018.1448001)

To link to this article: <https://doi.org/10.1080/09593330.2018.1448001>



Accepted author version posted online: 01 Mar 2018.
Published online: 08 Mar 2018.



Submit your article to this journal [↗](#)



Article views: 2



View related articles [↗](#)



View Crossmark data [↗](#)



CFD Investigation of the effects of bubble aerator layouts on hydrodynamics of an activated sludge channel reactor

Rainier Hreiz^a, Olivier Potier^b, Jim Wicks^b and Jean-Marc Commenge^a

^aLaboratoire Réactions et Génie des Procédés, Université de Lorraine, CNRS, LRGP, Nancy, France; ^bThe Fluid Group, The Magdalen Centre, Oxford, UK

ABSTRACT

In this paper, computational fluid dynamics (CFD) simulations are employed to characterize the effects of bubble aerator layouts (i.e. spatial arrangement) on the hydrodynamics in activated sludge (AS) reactors. The first configuration considered is a channel reactor with aerators placed alongside one lateral wall, for which velocity measurements are available in literature. CFD results were in good agreement with experimental data, which proves that the model is sufficiently accurate and predictive. Accordingly, simulations and numerical residence time distribution tests were conducted for different aerator layouts to determine their effects on the reactor hydrodynamics. The results revealed that the flow characteristics are extremely sensitive to the aerators arrangement given the high gas flow rates used in AS processes. Among the layouts investigated, the one where diffusers are placed all over the reactor floor has led to the least dispersive flow, i.e. which characteristics best tend toward that of an ideal plug flow reactor. Indeed, this flow field presented the lowest average turbulent diffusion and the most uniform axial velocity and turbulence fields. Such a flow behaviour is expected to be highly beneficial for biological treatment since it reduces pollutant dilution by axial diffusion and limits raw wastewater channelling to the outlet.

ARTICLE HISTORY

Received 11 January 2018
Accepted 1 March 2018

KEYWORDS

Activated sludge; CFD;
gas–liquid flow; RTD;
wastewater treatment

Nomenclature

C	Tracer concentration (mol kg^{-1})
D	Mass diffusivity ($\text{m}^2 \text{s}^{-1}$)
e	RTD function (s^{-1})
E	Dimensionless RTD function (–)
F	Force (N)
J	Number of reactors in series (–)
J^*	Nearest integer to J (–)
k	Turbulence kinetic energy ($\text{m}^2 \text{s}^{-2}$)
n_b	Number density of bubbles
P	Average pressure (N m^{-2})
Sc	Schmidt number (–)
t	Time (s)
\bar{t}	First central moment of the RTD (s)
Q	Volumetric flow rate ($\text{m}^3 \text{s}^{-1}$)
U	Average velocity (m s^{-1})
V	Volume (m^3)
y^+	Dimensionless wall ordinate (–)

Subscripts

D	For 'Drag force'
f	For 'Final'
g	For 'Gas'
l	For 'Liquid'
$lift$	For 'Lift force'
lub	For 'Wall-lubrication force'
t	For 'Turbulent'

Superscripts

o	For 'Outlet'
-----	--------------

1. Introduction

With the strengthening of environmental regulations and given the large expenses involved in wastewater treatment, a lot of research contributions have aimed at improving the design and operating conditions of activated sludge (AS) reactors. Special attention has been given to the aeration process since on the one hand it provides the necessary oxygenation for an efficient aerobic treatment, and on the other hand, it could represent more than 70% of the installation total power consumption [1].

Greek letters

α	Volume fraction (–)
θ	Dimensionless time (–)
μ	Dynamic viscosity (Pa s)
ρ	Density (kg m^{-3})
τ	Residence time (s)
σ^2	Second central moment of the RTD (s^2)

Hence, numerous studies employed mathematical optimization for determining the aeration policy (i.e. duration of aeration cycles and/or aeration intensity) that leads to the most cost-efficient treatment strategy. However, as noted in the literature review by Hreiz et al. [2], given the mathematical complexity that would arise from using partial differential equations in the process model, all these papers have overlooked the hydrodynamics effects and simply assumed an ideal flow pattern in the AS reactors. Nonetheless, the flow characteristics have definitely important effects on the treatment cost-effectiveness: (1) The hydrodynamics governs the liquid-to-flocs (e.g. nutrient uptake) and gas-to-liquid (e.g. oxygenation) mass transfer rates. Thus, it directly affects the process performance and operating costs. (2) The local concentrations of pollutant, dissolved oxygen and bacterial flocs, and hence the biochemical reactions rates, are widely affected by the flow characteristics. (3) Some designs and operating conditions may lead to the development of dead zones which reduce the reactor capacity and where sludge can accumulate over time (which may lead to local anaerobic conditions). (4) The competition between microorganisms with different growth rates is sensitive to the hydrodynamics conditions. For example, it has been reported that a flow field tending toward a plug flow behaviour favours zoogeal microorganisms while limiting the development of filamentous bacteria [3]. (5) Control systems of AS processes use local concentration measurements of dissolved species (oxygen, ammonia, etc.) as inputs. However, as a result of concentration gradients arising from incomplete mixing in the reactor, the location of the sensors can potentially affect the treatment effectiveness and cost [4].

Therefore, a considerable number of studies has been devoted to the characterization of the hydrodynamics in aerobic AS reactors. In this context, computational fluid dynamics (CFD) has been widely used as it allows quickly assessing the impact of the operating conditions and reactors design. For instance, Fayolle et al. [5] simulated the flow field and oxygen transfer in four wastewater reactors equipped with fine bubble diffusers. Their CFD results were in good agreement with velocity and oxygen transfer efficiency measurements. Le Moullec et al. [6] focused on the gas-liquid flow in a bench-scale channel reactor equipped with bubble aerators. Their CFD simulations were able to reproduce the velocity measurements data with good accuracy. Gresch et al. [7] investigated the effects of the aerator layouts on the hydrodynamics in aerobic reactors. Their results revealed that the flow characteristics are very sensitive to the diffusers arrangement. For additional details, the reader may refer to the literature review by Karpinska and Bridgeman

[8] or to Laurent et al. [9] and Wicklein et al. [10], which present recommendation for good modelling practice when applying CFD for simulating AS reactors.

As mentioned before, to the authors' knowledge, all studies considering the mathematical optimization of AS processes have relied on a systemic description of the reactors. This modelling approach neglects hydrodynamics phenomena (and focuses on biological reactions only), however, it requires moderate computational efforts only, which makes it suitable for conducting transient simulations. Hence, it allows characterizing the effects of the temporal variations of the wastewater composition and flow rate (due to the households' life-cycles or rain events for example) on the treatment efficiency. On the other hand, CFD simulations allow an accurate description of the flow field. However, given their computational expense, they have been used under steady-state operating conditions only.

In order to combine the advantages of both CFD and systemic simulations, some authors have employed the compartmental approach (e.g. [11,12]) or relied on residence time distribution (RTD) data to derive a flowsheet (i.e. arrangement of interconnected tanks) that reproduces the reactor's global hydrodynamics behaviour. The RTD curve may be acquired experimentally or numerically using the flow field calculated via CFD simulations. It can be exploited through various mathematical procedures to determine a flowsheet configuration allowing a fair representation of the flow phenomena in the bioreactor. For example, in many situations, the hydrodynamics in AS reactors can be adequately described using a model of continuous stirred tank reactors (CSTRs) in series (e.g. [13]). Based on the original RTD data, different techniques allow determining the number of tank reactors that would lead to a similar RTD curve (the reader may refer [14] for details). The flowsheet derived using such an approach constitutes a surrogate model that enables a satisfactory description of the reactor's global hydrodynamics behaviour, while being sufficiently straightforward to be employed in transient simulations (e.g. varying influent conditions) or used in model-based optimization of AS operation. It is noteworthy that when both experimental and numerical RTD are available, the average turbulent diffusivity in the reactor can be assessed by a fitting procedure (as discussed later in this paper). This step is fundamental for an accurate modelling of pollutant dispersion over the reactor in case where a biochemical model is to be coupled with the CFD approach.

In the present paper, the gas-liquid flow in a channel AS reactor equipped with bubble aerators is investigated via CFD simulations. Numerical results were in good agreement with the experimental data of Le Moullec

et al. [6]. As the CFD model proved to be sufficiently accurate and predictive, it has been employed to characterize the effects of the aerators spatial arrangement on the hydrodynamics in AS reactors. The results revealed that the flow field is extremely sensitive to the diffusers layout. RTD data showed that for most of the configurations investigated, the reactor's global hydrodynamics behaviour can be reasonably approximated through a model of CSTRs in series. The configuration where the reactor's floor is fully covered with porous diffusers engendered the lowest axial dispersion, i.e. the behaviour that best tends toward that of an ideal plug flow reactor. Such a flow field is desirable for providing high treatment efficiencies. Indeed, it limits the channelling of the raw wastewater to the outlet. Moreover, it ensures high biological reaction rates as it reduces the pollutant dilution by axial dispersion across the reactor.

2. Reactors configurations and operating conditions

The current study focuses on the influence of the aerators arrangement on the flow field in AS channel reactors using CFD. In order to evaluate the precision of the CFD model before any extrapolation, the geometric and operating conditions of the first configuration investigated were chosen so as to match those of a bench-scale reactor for which experimental measurements are reported [6]. Its dimensions are given in Figure 1. It corresponds to a channel reactor, i.e. its length is very long compared to its depth and width. A pipe with holes drilled each centimetre was used for bubbles injection. It was placed at the bottom of the reactor near a lateral wall. This configuration will be referred to as 'one-side aeration' along this manuscript.

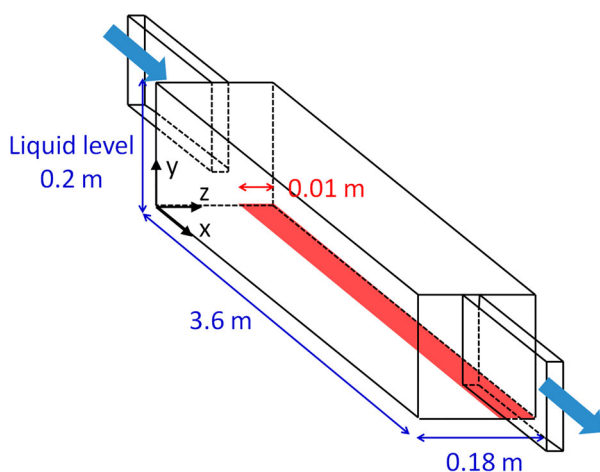


Figure 1. Schematic view of the AS reactor investigated by Le Moullec et al. [6] (not to scale). The red zone corresponds to the bubbles injection section used in CFD modelling.

Experiments were run using tap water with a flow rate of $0.216 \text{ m}^3 \text{ h}^{-1}$ and an air flow rate of $0.9 \text{ m}^3 \text{ h}^{-1}$. The average bubble size was estimated at 4 mm using photographic and double optical probe measurements. Liquid velocity was measured at different positions in the reactor using LDV (laser Doppler velocimetry). Supplementary information about this experimental study can be found in [6].

In addition to the 'one-side aeration' configuration (Figure 2(a)) for which experimental data are available, three other situations were investigated using CFD. They will be referred to as 'two-side aeration' (Figure 2(b)), 'central aeration' (Figure 2(c)) and 'full floor coverage' (Figure 2(d)) configuration respectively. The dimensions of these reactors and the gas and liquid flow rates are the same as those considered in the 'one-side aeration' layout: the only difference between these configurations is the bubble diffusers arrangement.

Similar bubble injection surfaces are used in the 'one-side', 'two-side' and 'central' aeration configurations in order to enable a meaningful characterization of the effects of the aerators layout. On the other hand, a larger injection zone is considered in the 'full floor coverage' layout where membrane diffusers are supposed to be placed over the whole reactor's floor: this configuration constitutes an ideal representation of a dense diffusers arrangement. Additional details about the aerators modelling are given in Sections 3.1 and 3.2.

3. CFD modelling of the gas-liquid flow in the reactors

3.1. Geometry and mesh

The geometry was drawn under ANSYS DesignModeler. The numerical domain is composed of the reactor

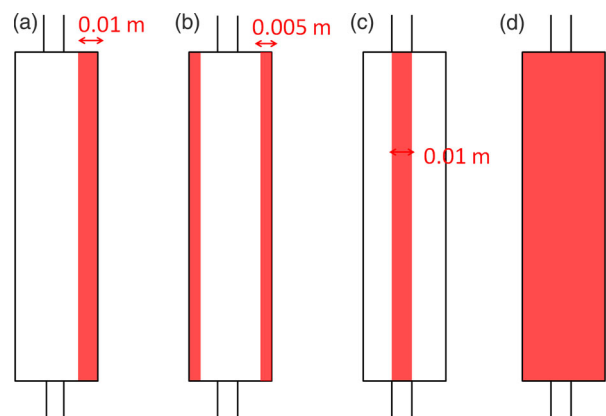


Figure 2. Top view of the different configurations investigated (not to scale): (a) 'One-side aeration' layout. (b) 'Two-side aeration' layout. (c) 'Central aeration' layout. (d) 'Full floor coverage' layout. The red zones correspond to the bubble injection sections used in CFD modelling.

section ($3.6 \times 0.18 \times 0.2 \text{ m}^3$, [Figure 1](#)) and an inlet (5 cm long, 1 cm wide and 12 cm high) and outlet (25 cm long, 1 cm wide and 12 cm high) channels. The length of the outlet was sufficient to avoid backflow issues that may arise in simulations. The height of the numerical domain is 20 cm, which corresponds to the water level in the reactor. The free surface is considered flat and horizontal.

For simplicity, the piping system used by Le Moulec et al. [6] for aeration is not integrated in the numerical domain. Instead, bubbles are supposed to be injected through a porous diffuser that is 1 cm wide and 3.6 m long in the ‘one-side aeration’ configuration ([Figure 2 \(a\)](#)). The same diffusers total surface is adopted in the ‘two-side’ ([Figure 2\(b\)](#)) and ‘central’ ([Figure 2\(c\)](#)) aeration layouts. Additional details about the aerators modelling are given in Section 3.3.

The numerical domain is discretized using a non-uniform Cartesian mesh (hexahedral elements). Grid refinement is adopted in the near-wall regions so as to obtain y^+ values lower than one as required by the turbulence model (see Section 3.2 for details). In the ‘two-side aeration’ geometry, fine cells are also used at the middle of the reactor where large gradients can be expected. Simulations were performed on different meshes. For the four configurations investigated, a mesh-independent solution was achieved using a mesh of about 7,00,000 cells.

3.2. Hydrodynamics modelling

The hydrodynamics modelling and simulation were performed using the ANSYS Fluent 16.1 commercial package [15]. The two-phase flow is considered isothermal and modelled using the full Euler-Euler approach (also known as two-fluid model). Both water and air phases are assumed incompressible and the interfacial mass transfer is neglected. The bubbles diameter is supposed constant. For each of the four configurations investigated, two simulations are run, the first one considering 1 mm diameter bubbles, and the second one adopting bubbles with an equivalent diameter (since they are not spherical) of 4 mm.

The mass balance equations for each phase give:

$$\rho_g \left[\frac{\partial(\alpha_g)}{\partial t} + \text{div}(\alpha_g \vec{U}_g) \right] = \text{div} \left(\frac{\mu_{t,g}}{0.75} \vec{\nabla}(\alpha_g) \right) \quad (1)$$

$$\rho_l \left[\frac{\partial(\alpha_l)}{\partial t} + \text{div}(\alpha_l \vec{U}_l) \right] = -\text{div} \left(\frac{\mu_{t,g}}{0.75} \vec{\nabla}(\alpha_g) \right) \quad (2)$$

where the subscripts g and l refer to the gas and liquid phases respectively, α is the local volume fraction (with $\alpha_g + \alpha_l = 1$), ρ the density and μ_t the turbulent viscosity.

\vec{U} is the average velocity which will be simply referred to as velocity in the remaining of the paper. The first term in each of Equations 1 and 2 corresponds to a temporal derivative and is taken zero when steady-state simulations are performed. The right hand side represents the turbulence dispersion force, which acts as a turbulent diffusion of the dispersed phase [16].

Using Boussinesq’s eddy viscosity concept, the momentum conservation gives:

$$\rho_i \left[\frac{\partial(\alpha_i \vec{U}_i)}{\partial t} + \text{div}(\alpha_i \vec{U}_i \otimes \vec{U}_i) \right] = -\alpha_i \vec{\nabla}(P) + \alpha_i \rho_i \vec{g} \quad (3)$$

$$+ \vec{\text{div}} \left[\alpha_i (\mu_{t,i} + \mu_i) (\vec{\nabla} \vec{U}_i + \vec{\nabla} \vec{U}_i^T) - \frac{2}{3} \alpha_i \rho_i k_i \vec{1} \right] + \vec{F}_i$$

where the subscript i refers to one phase (gas or liquid), P is the averaged pressure (shared by the two phases), μ the molecular viscosity, k the turbulence kinetic energy and \vec{F} the interaction forces (per unit volume) between the phases. The first term in Equation 3 is a temporal derivative and thus is taken zero when steady-state simulations are performed.

The interphase momentum transfer per unit volume, \vec{F} , equals the force exerted on/by a single bubble, multiplied by the number density of bubbles in the considered computational cell, n_b (which is easily calculated from α_g since the bubbles diameter is known):

$$\vec{F}_g = -\vec{F}_l = n_b (\vec{F}_D + \vec{F}_{lift} + \vec{F}_{lub}) \quad (4)$$

As shown in Eq. 4, three interaction forces are considered in the present model. \vec{F}_D is the drag force. The drag coefficient is modelled following the model of Clift et al. [17], which is valid for spherical and non-spherical bubbles. \vec{F}_{lift} is the lift force. The lift coefficient was calculated using the Moraga et al. model [18]. \vec{F}_{lub} is the wall-lubrication (or wall-induced lift) force. It acts in the immediate vicinity of the wall only, and pushes the bubbles laterally away from the wall. The virtual mass force was not included in the model. Indeed, in this paper, the focus is put on the permanent flow regime, where this force is expected to have small effects only (since it is mainly significant in rapid transient flows). Moreover, its addition to the model often gives rise to convergence issues.

The turbulent viscosity of the liquid phase is calculated using the well-known k - ω shear stress transport (SST) turbulence model. On the other hand, the turbulence characteristics of the dispersed phase were not calculated through transport equations but using Tchen’s theory.

The bubble-induced turbulence was dealt with via the Troshko and Hassan model [19]. This model, which was developed for bubbly flows, considers supplementary source terms in the transport equations of k_l and ω_l to

account for bubbles modulation of the liquid turbulence. It is extremely important to consider the bubble-induced turbulence effect when dealing with aerated AS reactors. Indeed, in such processes, the gas flow rate is usually very large to provide sufficient oxygenation, while the liquid velocity is relatively low to guarantee a convenient residence time in the reactor. Therefore, the momentum and turbulence induced by the bubbles can be much more important than those due to the liquid flow. For example, in the case of the bench-scale reactors investigated in this study, the liquid Reynolds number is about 316, which indicates that, in absence of bubble injection, the flow would be laminar. However, as shown experimentally in [6], the two-phase flow is very turbulent due to bubbles effects.

Concerning the near-wall regions, as indicated in Section 3.1, a fine mesh is used on all wall boundaries to guarantee y^+ values less than one. Thus, the turbulence model can be integrated all over the boundary layer to the wall. This modelling approach is computationally much more expensive than the use of the law of the wall. However, since turbulence in bench-scale reactors is thoroughly due to bubbles as noted previously, this modelling strategy is probably more accurate.

3.3. Boundary conditions and bubbles injection procedure

A uniform velocity condition is set at the reactor inlet where only water is present. A uniform pressure condition is imposed at the reactor outlet and a no slip condition at the walls. A 'degassing' condition is applied on the free surface which is considered flat, horizontal and non-deformable. Thus, it acts as a zero-shear stress boundary condition for the liquid phase while allowing bubbles to escape through.

For simplicity, aeration is performed through the whole surface of the diffusers and not only through the aeration pores. Otherwise, all the individual pores have to be drawn and meshed. In literature studies (e.g. [6]), an inlet boundary condition is set at the diffusers surface: it allows gas injection at a chosen flow rate while imposing a zero velocity condition to the liquid phase. However, although the liquid velocity is taken zero, commercial CFD codes do not regard this surface as a 'wall condition' for the liquid phase. This leads to erroneous estimations of the liquid turbulence characteristics in the cells adjacent to the diffuser (and even of the wall shear stress in some cases). Indeed, holes occupy only a moderate fraction of the porous membrane. Therefore, it would be more appropriate to set a 'wall' boundary condition for the liquid phase at the aerators position. Moreover, the use of

an inlet-type boundary condition requires specifying the gas volume fraction value at the membrane surface, which is however an unknown feature of the problem.

In order to avoid the limitations of this approach, a more convenient modelling strategy is adopted in this paper. A wall condition is assigned to the whole diffusers surface so as to provide a correct boundary condition for the liquid phase. However, the use of a wall condition does not enable injecting the bubbles into the domain via this boundary. Therefore, instead, bubbles are generated within the computational domain, in a thin volume of 1 mm thickness just above the diffusers. This is achieved through the addition of a constant volumetric mass source term in Equation 1: this term is non zero in the thin bubbles generation domain only, and its value is chosen so as to match the experimental air flow rate. Thus, using this strategy, bubbles are created in the immediate vicinity of the diffusers to which a wall condition is assigned, guaranteeing hence an appropriate near wall modelling.

3.4. Numerical schemes and solver

The convective terms in Equations (1–3) were discretized using the QUICK scheme while diffusive terms were central-differenced. Pressure interpolation was carried out using a second order scheme.

The hydrodynamics equations were solved using a steady-state coupled solver. However, convergence could be achieved for the 'one-side aeration' case only. Indeed, for the three remaining configurations, the permanent flow regime revealed to be unsteady. Therefore, these simulations were solved transiently. Advancement in time was achieved through a second-order implicit scheme until reaching the permanent flow regime. From that point onward, the variables values were averaged so as to calculate the mean flow characteristics. A time step of 0.004 s was used in the case of the 'central' and 'two-side' aeration arrangements, while a time step of 0.01 s was sufficient with the 'full floor coverage' configuration which involves lower velocities (given its large bubble injection section) as well as lower fluctuations of the mean velocity field (refer to Section 4 for details).

3.5. RTD simulations

The numerical RTD curves are derived by injecting a pulse input of a tracer (i.e. a passive scalar) at the reactor inlet, and monitoring the tracer concentration at the reactor outlet as a function of time. The tracer has the same physical properties than water and is

allowed to diffuse within the liquid phase only. The transport equation of the tracer concentration is:

$$\frac{\partial(\alpha_l \rho_l C_l)}{\partial t} + \text{div}(\alpha_l \rho_l \vec{U}_l C_l) = \text{div} \left[\alpha_l \left(\rho_l D_l + \frac{\mu_{t,l}}{Sc_{t,l}} \right) \vec{\nabla}(C_l) \right] \quad (5)$$

where C_l is the tracer concentration per unit mass of liquid, D_l is the molecular diffusivity of the tracer in the liquid and $Sc_{t,l}$ is the liquid turbulent Schmidt number. D_l is taken as $10^{-9} \text{ m}^2 \text{ s}^{-1}$ which corresponds to a typical order of magnitude of diffusivities in liquids. However, since the flow is sufficiently turbulent (as confirmed by the simulations results), its value has negligible effects on the RTD curve. Indeed, the tracer diffusion is generally governed by turbulence effects.

Therefore, a convenient estimation of the turbulent Schmidt number (and of the local turbulent viscosity) is required. Although the value of $Sc_{t,l}$ probably depends on the local flow characteristics, as noted in the literature review by Gualtieri et al. [20], in CFD simulations, it is generally assumed constant over the whole computational domain. Moreover, based on experimental RTD results, the best-fitting $Sc_{t,l}$ seems to be case-dependent. It generally varies between 0.1 and 1 [20], which is a relatively large range since the results may be very sensitive to its value. In this paper, $Sc_{t,l}$ was set in all simulations to 0.8, a value commonly used when dealing with bubbly flows.

In the case of the 'one-side aeration' layout, as mentioned before, a steady-state hydrodynamics solution could be achieved. Therefore, to compute the RTD curve, this steady-state flow field was used, and only Equation 5 was integrated in time with a 1 s time step. On the other hand, in the three other reactor configurations, the permanent flow regime was unsteady. Thus, it is necessary to integrate Equation 5 together with Equations (1–3) in order to obtain the exact RTD curve, which may also depend on the tracer injection time. However, the hydrodynamics equations require a small integration time step (Section 3.2) while Equation 5 needs to be integrated over a large time frame of several thousands of seconds. Thus, the computation of the exact RTD data requires extensive computational time.

In order to avoid this issue, three RTD sets were performed for each of these configurations by integrating Equation 5 only (which allows using relatively large time steps), but starting at different – arbitrarily chosen – initial times, i.e. by using different flow field conditions. However, it is noteworthy that this procedure may underestimate the diffusion rate in the reactor since the tracer dispersion due the time-varying velocity conditions is not accounted for. Time integration was achieved using a second order scheme with a time

step of 1 s in the 'full floor coverage' case and 0.5 s in the 'two-side' and 'central' aeration cases.

In this paper, the reactor global hydrodynamics behaviour is modelled using the CSTRs in series approach. This model has a single parameter, J , the number of tanks (which all have the same volume). The RTD data acquired on the AS reactor are analyzed so as to determine the value of J leading to the RTD that best approaches the original one. First, the RTD function, $e(t)$, is calculated as follows:

$$e(t) = \frac{C_l^o(t)}{\int_0^{t_f} C_l^o(t) dt} \quad (6)$$

with $t = 0$ corresponding to the pulse injection time. C_l^o is the average tracer concentration at the reactor outlet as a function of time. t_f is the duration of data acquisition. It should be sufficiently large to ensure that most of the tracer is discharged before stopping data monitoring, i.e. that C_l^o is negligible at t_f .

The first central moment of the distribution, \bar{t} , gives the average liquid residence time. It is calculated as follows:

$$\bar{t} = \int_0^{t_f} t e(t) dt \quad (7)$$

The second central moment, σ^2 , indicates the variance of the distribution. It is calculated as follows:

$$\sigma^2 = \int_0^{t_f} (t - \bar{t})^2 e(t) dt \quad (8)$$

The number of CSTRs in series, J , is obtained from the moment ratio:

$$J = \frac{\bar{t}^2}{\sigma^2} \quad (9)$$

For generality purposes, it is preferred to represent the RTD curves using dimensionless variables. Thus, the dimensionless time, θ , is used instead of t :

$$\theta = \frac{t}{\tau_l} \quad (10)$$

where τ_l is the liquid residence time that would be obtained in the absence of dead zones within the reactor. Since the reactor mainly contains water (i.e. the gas fraction is negligible compared to that of liquid), τ_l can be calculated as follows:

$$\tau_l = \frac{V}{Q_l} \quad (11)$$

where V is the total reactor volume and Q_l the liquid volumetric flow rate. Concerning the RTD function $e(t)$, it is put into dimensionless form as follows:

$$E(t) = \tau_l e(t) \quad (12)$$

4. Hydrodynamics results and discussion

In this section, results related to the hydrodynamics and flow behaviour in the different reactors are presented. It is worthy to recall that the same gas and liquid flow rates are used in all of the layouts investigated: the only difference between these configurations is the bubble diffusers arrangement.

4.1. 'One-side aeration' configuration

The 'one-side aeration' layout has led to a steady-state flow field in both cases where 4 mm or 1 mm bubbles were considered. The results reveal that, apart in the vicinity of the inlet and outlet channels, the flow is practically invariant along the reactor length (i.e. x direction, Figure 1).

Figure 3(a) shows the liquid velocity vectors in the vertical mid-plane (i.e. located at $x = 1.8$ m) in the case of 4 mm bubbles. The rising bubbles drag the liquid upward near the right lateral wall (where the diffuser is placed). Once they reach the free surface, bubbles disengage, while the liquid turns over and then moves downward at the non-aerated wall side, which leads to a large recirculation cell. The liquid y - and z -velocity components, which are induced by the air flow, are much larger than the x -velocity. At the reactor's non-aerated corner, a small recirculation loop forms. This flow feature is probably undesirable as it may lead to sludge accumulation and to a possible inhibition of the biochemical reactions due to locally low oxygen concentrations.

In the case of 1 mm bubbles, a similar flow pattern is observed. However, the maximum liquid vertical velocity slightly exceeds 0.29 m s^{-1} , while it is about 0.2 m s^{-1} only in the case of 4 mm bubbles. Concerning the bubbles velocity, as expected, large bubbles rise faster than smaller ones. The bubbles maximum rise velocity

is about 0.39 m s^{-1} in the case of 1 mm bubbles, while it nearly reaches 0.45 m s^{-1} in the case of 4 mm bubbles. So despite the fact that 1 mm bubbles rise slower than the 4 mm ones, they do lead to higher liquid velocities. This effect can be explained by the fact that, given their significant surface to volume ratio, fine bubbles exert a greater drag on liquid which leads to a more efficient gas-lift (and lower slip velocities).

Figures 4(a–c) compare liquid velocity measurements [6] to the current CFD results obtained using 4 mm bubbles, which correspond to the average bubble size evaluated experimentally. Despite the numerous assumptions used in the model (uniform and steady gas injection, uniform bubble size, etc.), a very good agreement is obtained between experimental and numerical results: the simulation reliably reproduced the mean flow field characteristics. Therefore, CFD results obtained with the remaining reactor configurations (for which no experimental data are available) can be expected to be relatively trustworthy.

The air volume fraction in the vertical mid-plane in the case of 4 mm bubbles is shown in Figure 3(b). The rising bubbles form a curtain which thickness slightly increases along the upward vertical direction, until the vicinity of the free surface is reached. There, the widening of the bubbles curtain becomes more pronounced since bubbles are dragged toward the centre of the reactor by the horizontally flowing liquid (Figure 3(a)). As it could be seen from Figure 3(b), the inclusion of the wall-lubrication force in the model prevents 'artificial' bubbles accumulation over the wall as it pushes the bubbles laterally away toward the bulk flow.

In the case of 1 mm bubbles, a qualitatively similar air fraction field is obtained. As small bubbles rise slower than larger ones, higher void fractions are observed, reaching about 5.9% near the aerator. The initial thickness of the bubble curtain is slightly lower than in the

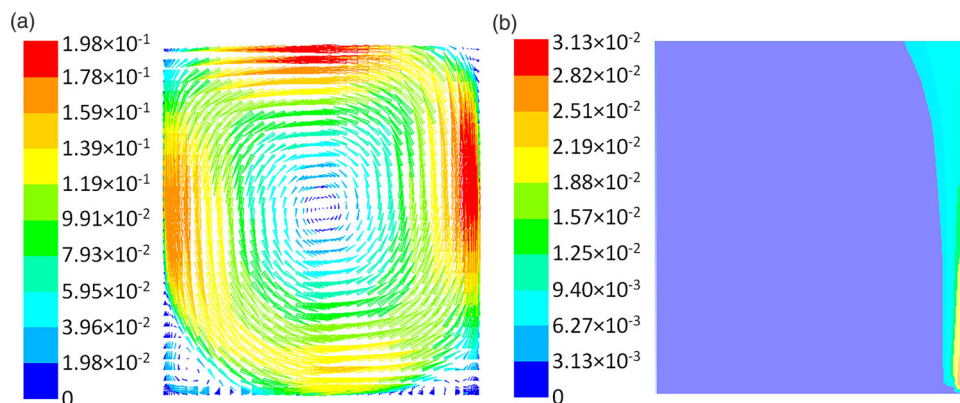


Figure 3. One-side aeration' flow field characteristics in the vertical mid-plane (numerical results, 4 mm bubbles case): (a) Liquid velocity vectors coloured according to their magnitude in m s^{-1} . (b) Gas fraction contour plot.

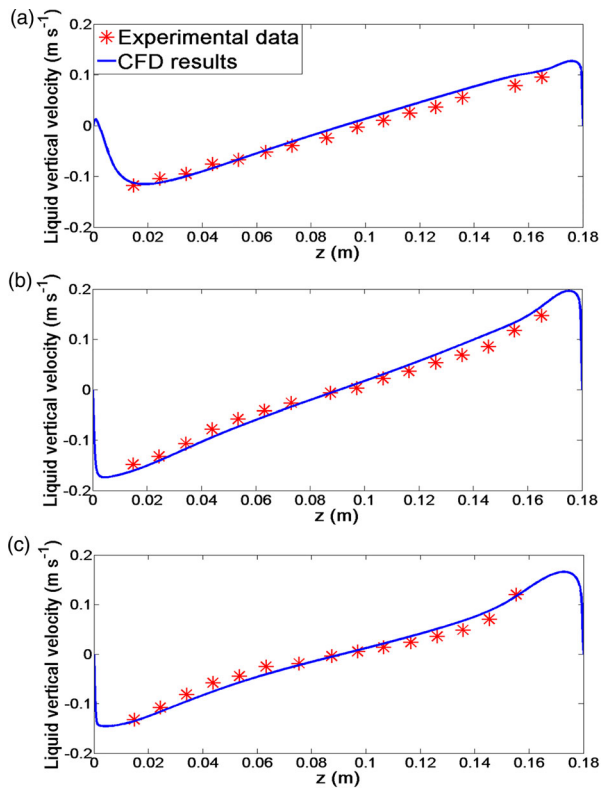


Figure 4. Comparison between liquid velocity measurements by Le Moullec et al. [6] (averaged) and CFD results (using 4 mm bubbles) in the ‘one-side aeration’ configuration: (a) at $y = 50$ mm. (b) at $y = 100$ mm. (c) at $y = 150$ mm.

case of 4 mm bubbles. However, in the vicinity of the free surface, bubbles are carried deeper toward the centre of the reactor. This is due to the higher liquid horizontal velocities in the case of 1 mm bubbles as well as the fact that small bubbles are more easily dragged than larger ones.

4.2. ‘Two-side aeration’ configuration

In the case of the ‘two-side aeration’ layout, bubbles form two curtains that move upward along the lateral walls

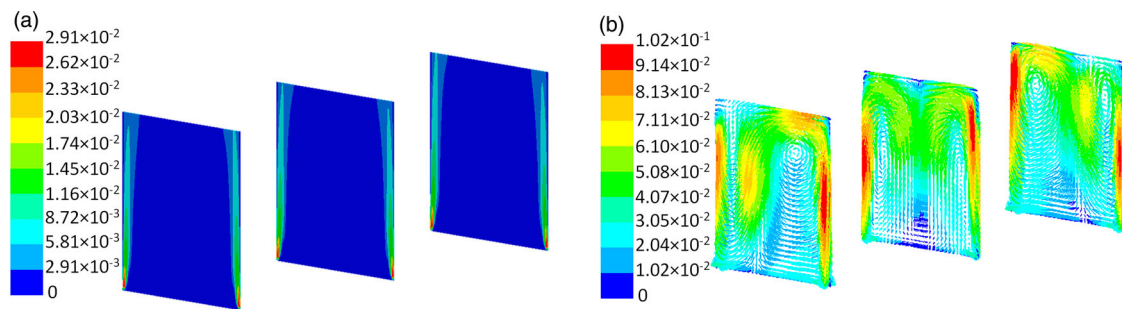


Figure 5. ‘Two-side aeration’ flow field characteristics – at an arbitrary chosen time – in the vertical planes (from left to right) $x = 2.05$ m, 1.8 m and 1.55 m (numerical results, 4 mm bubbles case): (a) Gas fraction contour plot. (b) Liquid velocity vectors coloured according to their magnitude in m s^{-1} .

(Figure 5(a)). Higher void fractions are observed in the case of 1 mm bubbles which rise slower than the 4 mm ones. Although the void fraction field seems to be as symmetrical as the flow generating conditions, the flow field engendered presents a loss of symmetry as shown in Figure 5(b). Liquid is dragged upward by the bubble curtains, turns around at the free surface and then moves downward, creating two recirculation cells as it could be expected. However, liquid downwelling does not occur at the middle of the reactor section: the zone of descending liquid presents spatial oscillations along the x direction. Moreover, it undergoes local temporal oscillations. In the case of 1 mm bubbles, the flow gets more unstable, and the magnitudes of both temporal and spatial oscillations become higher.

The results presented in this paragraph emphasize the fact that, even in the case of symmetrical flow generating conditions, the simulations should be performed over the whole reactor volume (instead of considering half of the domain with an imposed symmetry boundary condition). Otherwise, they will not be able to predict the occurrence of such instability. However, it is noteworthy that the development of this instability is probably not inherent to the ‘two-side aeration’ layout. Indeed, its occurrence is expected to depend on the flow rates (and physical properties) of the gaseous and liquid phases, the bubble size and the dimensions and geometry of the flow section.

4.3. ‘Central aeration’ configuration

As in the ‘two-side aeration’ case, the simulations revealed that the ‘central aeration’ layout leads to a symmetry-breaking phenomenon in both cases where 1 mm or 4 mm bubbles are considered. Indeed, as shown in Figure 6(a) the bubble plume does not rise vertically, but adopts a curved shape which curvature presents spatial oscillations along the x direction. The plume expands along the vertical direction due to turbulent

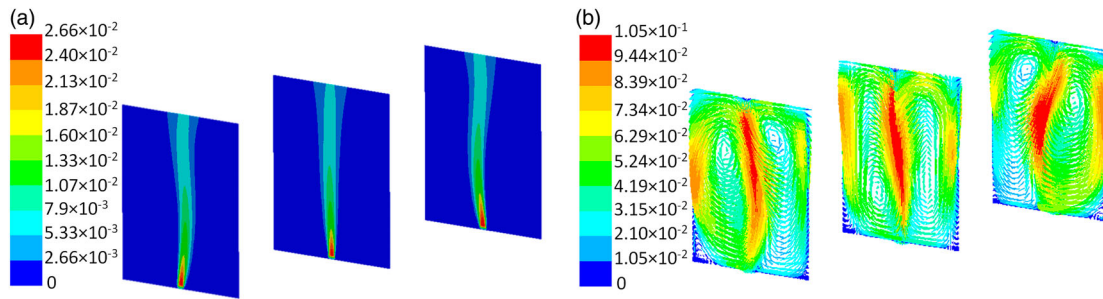


Figure 6. 'Central aeration' flow field characteristics – at an arbitrary chosen time – in the vertical planes (from left to right) $x = 2.05$ m, 1.8 m and 1.55 m (numerical results, 4 mm bubbles case): (a) Gas fraction contour plot. (b) Liquid velocity vectors coloured according to their magnitude in m s^{-1} .

diffusion. Figure 6(b) shows that the liquid phase is dragged upward within the bubble plume and tends to move downward near the lateral walls. However, the flow field is chaotic and several recirculation cells are generally present in the vertical flow sections, especially in the case of 1 mm bubbles.

Moreover, the flow is unsteady and the bubble panache slightly oscillates around its mean position. The flow field gets more disorganized when 1 mm bubbles are used: the frequency and magnitude of the plume's temporal and spatial oscillations, as well as its curvature, are higher than in the case of 4 mm bubbles. Finally, it is noteworthy that this wavy and oscillating bubble plume phenomenon is encountered in bubble columns equipped with a central aeration system [21,22].

4.4. 'Full floor coverage' configuration

As mentioned before, no steady-state solution could be obtained in the 'full floor coverage' configuration. However, although the permanent regime is unsteady,

the mean flow exhibits slight fluctuations only. Thus, the solution may be regarded as quasi-steady.

Figures 7(a) and 8(a) show void fraction contour plots in the 4 mm and 1 mm bubbles cases respectively. Given the uniform aeration conditions, bubbles are homogeneously dispersed in the bulk flow all over the reactor. However, zones of low gas fraction lie in the immediate vicinity of the lateral walls. They are mostly noticeable in the 4 mm bubbles case. These zones are due to the wall-lubrication force that pushes bubbles laterally away from the walls, which results in relatively high void fractions in the adjacent layers.

Concerning the liquid flow field, in the case of 4 mm bubbles, it is practically symmetric (Figure 7(b)) and invariant in the x direction (apart in the vicinity of the inlet and outlet channels). The flow gets organized in two large recirculation patterns with ascending velocities near the lateral walls and liquid downwelling at the middle of the flow section. The simulation predicts the development of two narrow recirculation cells near the lateral walls. However, the occurrence of these flow structures is not necessarily physical. They could be

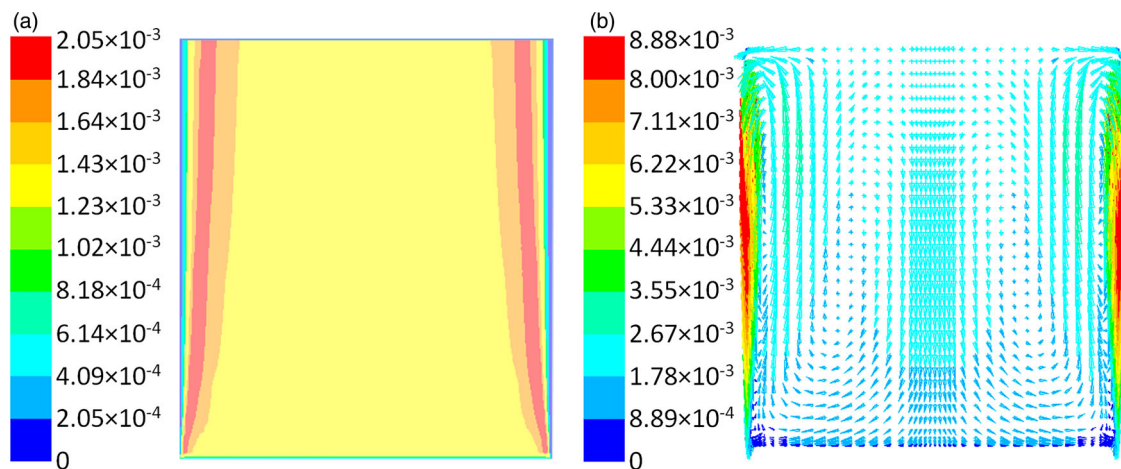


Figure 7. 'Full floor coverage' flow field characteristics – at an arbitrary chosen time – in the vertical mid-plane (numerical results, 4 mm bubbles case): (a) Gas fraction contour plot. (b) Liquid velocity vectors coloured according to their magnitude in m s^{-1} .

due to the modelling procedure of the wall-lubrication force which pushes the bubbles too much away from the wall as it can be seen from [Figure 7\(a\)](#).

Liquid and bubbles velocities are much lower in the ‘full floor coverage’ configuration than in the previously investigated layouts. Indeed, its much larger diffuser surface leads to lower bubble injection velocities. Moreover, since bubbles are spread all over the reactor, ‘swarming’ effects are reduced which limits the bubbles (and hence the liquid) rise velocity.

When 1 mm bubbles are used, the symmetry of the flow field is broken. The velocity field obtained ([Figure 8\(b\)](#)) involves two recirculation cells where liquid moves upward in the vicinity of the lateral walls. The zone of liquid downwelling presents spatial oscillations along the x direction. However, the flow remains quasi-steady, i.e. the mean flow exhibits slight fluctuations only, although their magnitudes are higher than in the 4 mm bubbles case.

4.5. Average void fraction

The gas fraction in aerobic AS reactors is a crucial parameter for characterizing the process efficiency since it is positively correlated to bubbles contact time and oxygen transfer rate. The average void fractions in the different reactors investigated are reported in [Table 1](#). Values related to the ‘one-side aeration’ configuration, for which a steady-state solution was determined, were calculated by spatially averaging the steady-state void fraction over the reactor volume. The remaining results correspond to a spatial and temporal averaging of the gas fraction during the unsteady permanent regime.

As it could be expected, regardless of the aerators layout, 1 mm bubbles generate higher void fractions since fine bubbles rise slower than larger ones. Moreover, given their higher surface to volume ratio, they lead to a much greater interfacial area. So from an oxygenation point of view, fine bubble diffusers are considerably more efficient than coarse bubble aerators.

Table 1. Average air fraction depending on the aerators layout.

	‘One-side aeration’	‘Two-side aeration’	‘Central aeration’	‘Full floor coverage’
1 mm bubbles	1.54×10^{-3}	1.99×10^{-3}	2.18×10^{-3}	3.39×10^{-3}
4 mm bubbles	1.07×10^{-3}	1.26×10^{-3}	1.27×10^{-3}	1.55×10^{-3}

For both bubble sizes investigated, the ‘one-side’ aeration leads to the lowest average air fraction ([Table 1](#)). Indeed, as bubbles are injected at the same location, they rise faster due to ‘swarm’ effects: as it can be seen from [Figures 3\(a\)](#), [5\(b\)](#), [6\(b\)](#) and [7\(b\)](#), this layout leads to the highest liquid (and bubbles) rise velocity. Moreover, compared to the bulk flow, the liquid within the bubble curtain is expected to be relatively concentrated in oxygen which should lead to a decrease in the bubble-to-liquid oxygen transfer rate. On the other hand, the ‘full floor coverage’ configuration generates the highest air fractions. Indeed, given the uniform gas injection conditions, bubbles are homogeneously dispersed within the reactor and thus, they rise slowly. Moreover, such a homogenous bubbles distribution ensures a more uniform oxygen supply over the reactor and avoids dead and anoxic zones.

Therefore, it can be expected that the ‘full floor coverage’ configuration leads to appreciably better oxygenation performance than the other aerators layouts. However, it should be underlined that the analysis exposed above neglects some significant flow phenomena. For example, it has been assumed in the simulations that the bubble size does not depend on the liquid flow field or on the bubbles injection velocity. Moreover, the effects of the liquid turbulence on the mass transfer rate have not been accounted for. Indeed, the ‘one-side’, ‘two-side’ and ‘central’ aeration configurations involve high turbulence levels around the bubble swarms, which enhance gas–liquid mass transfer. Therefore, in order to quantify the aeration effectiveness, additional transport equations (for the gaseous and dissolved oxygen) and closure terms (evaluation of the

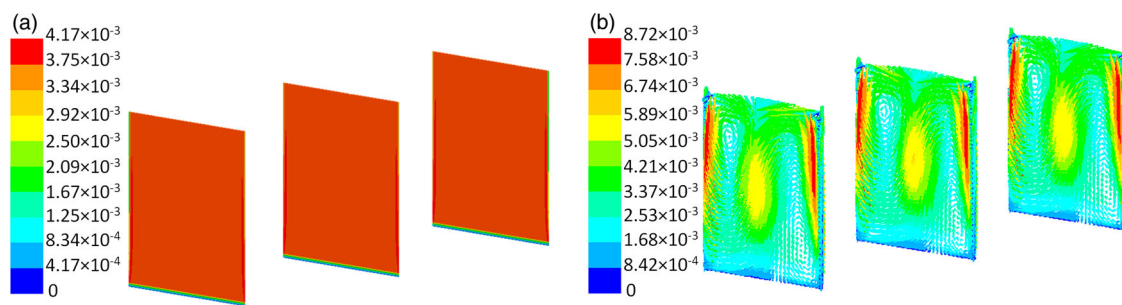


Figure 8. ‘Full floor coverage’ flow field characteristics – at an arbitrary chosen time – in the vertical planes (from left to right) $x = 2.05$ m, 1.8 m and 1.55 m (numerical results, 1 mm bubbles case): (a) Gas fraction contour plot. (b) Liquid velocity vectors coloured according to their magnitude in m s^{-1} .

interfacial mass transfer coefficient, etc.) should be considered in the CFD model.

5. RTD results and discussion

The number of CSTRs in series, J , allowing the best representation of the reactors global hydrodynamics behaviour is reported in Table 2 for the different aerator layouts investigated. For each bubble size, three values are given in the case of the 'two-side', 'central' and 'full floor coverage' configurations. Indeed, as explained in Section 3.5, three RTDs were performed in these situations for which no steady-state solution could be determined.

The RTD curves obtained using CFD and the best-fitting CSTRs in series model (J^* being the nearest integer to J) are compared in Figure 9 for several cases. The RTD data of the systemic model are calculated as follows:

$$E(t) = \left(\frac{J^*}{\tau_l}\right)^{J^*} \frac{t^{(J^*-1)} \exp(-J^* \theta)}{(J^* - 1)!} \tau_l \quad (13)$$

The narrower the RTD curve (i.e. low variance, σ^2), the higher the number of equivalent CSTRs in series J , and therefore the behaviour of the AS reactor tends more toward that of an ideal plug flow. On the other hand, a broad RTD curve indicates a flow behaviour engendering high axial dispersion. The tracer dispersion results from several effects: (a) Non-uniformity of the axial velocity field. (b) Molecular diffusion whose influence is however negligible as the flow is turbulent. (c) Turbulent diffusion whose effects depend on the selected value of $Sc_{t,l}$ (0.8 in the current study). (d) Numerical diffusion which is supposed insignificant as a fine mesh and a small time step are used. (e) Non-uniformity of the turbulent diffusion field. This effect is limited in the 'full floor coverage' layouts as shown in Figure 10(a) (the turbulent diffusion field gets even more uniform in the case of 1 mm bubbles). On the contrary, the remaining configurations engender zones of significantly high turbulent diffusivities: at the centre of the reactor in the case of the 'one-side aeration' layout (Figure 10(b)), and around the bubble plume in the 'central' and 'two-side' aeration configurations.

Table 2. Number of reactors, J , leading to the best fit between the CSTRs in series model and the CFD RTD curves.

	'One-side aeration'	'Two-side aeration'	'Central aeration'	'Full floor coverage'
4 mm bubbles	15.5	10.3	9.1	30.1
		10.3	10.3	29.7
		10.3	9.6	30.1
1 mm bubbles	12.0	16.3	6.7	50.5
		13.3	3.9	50.8
		14.5	5.2	50.9

It is noteworthy that the global hydrodynamic behaviour engendered by the different aerators layouts can be fairly represented by the CSTRs in series model (Figure 9), although a relative discrepancy is observed. These differences are potentially due to the 3D nature of the flow, the presence of recirculation cells, the important velocity gradients and the inhomogeneous turbulent diffusion field, etc. Accordingly, the compartmental approach can be used to derive a more accurate surrogate model than the CSTRs in series if desired.

5.1. Comparison with experimental data

The comparison with the experimental RTD (results not shown here) of Le Moullec et al. [6] ('one-side aeration' layout) reveals that the numerical RTD underestimates dispersion effects in the reactor. Indeed, the number of CSTRs in series allowing the best fit to experimental data was found to be about 6.8, which is much lower than $J = 15.5$ (Table 2) predicted by the simulation.

This inconsistency is presumably due to the value assigned to $Sc_{t,l}$, 0.8. In fact, Le Moullec et al. [6] have shown that, in the 'one-side aeration' layout, the tracer dispersion is mainly due to turbulence effects. Therefore, a lower value of $Sc_{t,l}$ should lead to better agreement with experimental data. Other potential reasons behind the disagreement between CFD and experiments are the inaccuracies in the predicted turbulent viscosity field, and the assumptions of uniform $Sc_{t,l}$, steady and uniform aeration and monodisperse bubbles, etc.

As mentioned before, all the RTDs performed in this study were conducted using a $Sc_{t,l}$ of 0.8. Nevertheless, as discussed in Section 5.3, the comparison of the different RTD curves stills meaningful and allows drawing interesting conclusions about the effects of the aerators layout on the global flow behaviour.

5.2. Effects of the bubbles size

The results reported in Table 2 reveal that the bubble size does not have a regular effect on the global dispersion coefficient in the reactor. In fact, large bubbles lead to a more dispersive flow in the 'two-side aeration' and 'full floor coverage' configurations, while the opposite effect is observed in the case of the 'one-side' and 'central' aeration layouts.

Actually, the effects of the bubble size on the global flow behaviour seem to be quite complex. Indeed, large bubbles lead to a greater bubble-induced turbulence than smaller ones. However, fine bubbles were observed to generate higher liquid velocities and a more chaotic flow, which engenders more shear-

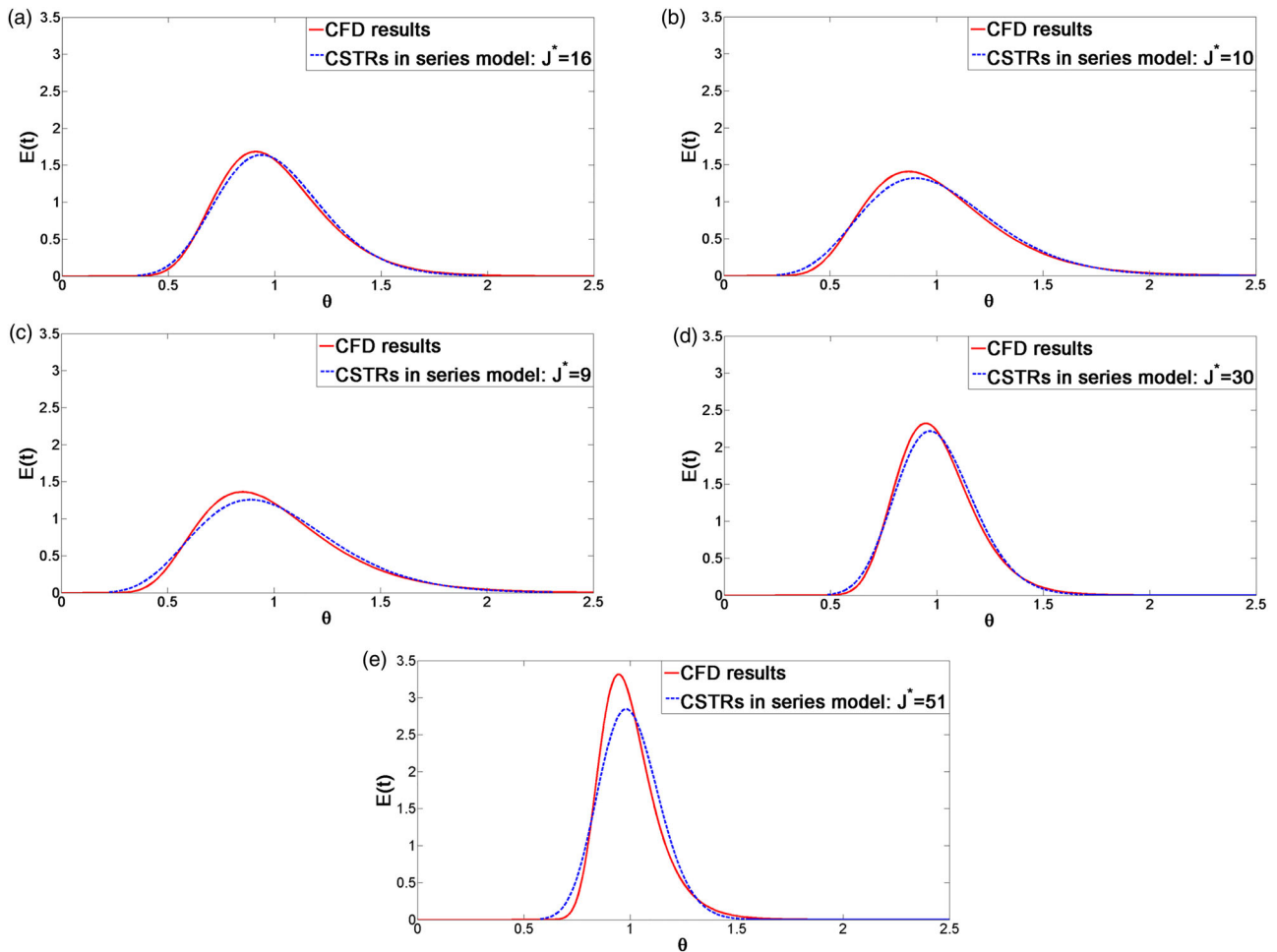


Figure 9. RTD curves obtained via CFD simulations and the best-fitting CSTRs in series model: (a) ‘One-side aeration’ with 4 mm bubbles. (b) ‘Two-side aeration’ with 4 mm bubbles. (c) ‘Central aeration’ with 4 mm bubbles. (d) ‘Full floor coverage’ with 4 mm bubbles. (e) ‘Full floor coverage’ with 1 mm bubbles.

induced (i.e. classic) turbulence. Thus, the overall effect of the bubble size is case-dependent given that the rate of turbulence generation may be very sensitive to the flow characteristics.

5.3. Effects of the aerators pattern

The results presented in Table 2 (and Figure 9) reveal that, by far, the ‘full floor coverage’ layout generates the hydrodynamics behaviour that best tends toward

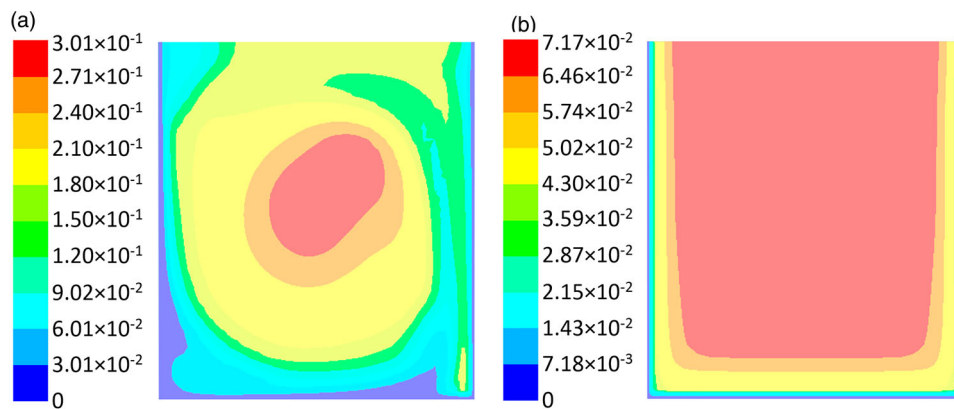


Figure 10. Contour plots of the liquid turbulent diffusion coefficient in the vertical mid-plane (in $m^2 s^{-1}$): (a) ‘Full floor coverage’ layout with 4 mm bubbles. (b) ‘One-side aeration’ layout with 4 mm bubbles. Note that different colour scales are used in the two figures.

that of an ideal plug flow reactor, i.e. that is described by the greater number of CSTRs in series. Such a flow field is desirable for providing a high treatment efficiency: (a) It limits the channelling of raw wastewater to the outlet, and hence, ensures an adequate retention time for all the liquid parcels. (b) It allows high biological reaction rates as it reduces pollutant dilution by axial diffusion across the reactor. (c) It favours the development of zoogeal microorganisms at the expense of filamentous bacteria [3]. It should be underlined that in the 'full floor coverage' layout, as the flow is quasi-steady, the three RTDs performed have led to very similar results.

In an attempt to relate the equivalent number CSTRs, J , to the turbulent characteristics of the flow, the average diffusion coefficient in the reactor has been calculated. However, no regular relationship between the two entities could be found. Indeed, the flow non-uniformity seems to have a significant impact on the overall dispersion coefficient, especially in the case of the 'two-side' and 'central' aeration layouts where the flow is very chaotic (however, the influence of the flow non-uniformity will be reduced compared to the effects of turbulent diffusion if a lower value is used for $Sc_{t,l}$). Moreover, as mentioned previously, the tracer dispersion does probably not depend on the average turbulent diffusion only, but also on the turbulence field which is far from being uniform apart from the case of the 'full floor coverage' layout.

In any case, the 'full floor coverage' engenders the lowest average turbulent diffusion, and the most uniform axial velocity and turbulence fields. Therefore, as the best-fitting $Sc_{t,l}$ is expected to not vary much apart from one reactor configuration to another, the simulation results indicate that the 'full floor coverage' layout leads to the flow that best approaches the plug flow behaviour, regardless of the fact that the $Sc_{t,l}$ value used in this paper did not allow a precise match of the experimental RTD data.

6. Conclusion and perspectives

In this paper, CFD simulations and numerical RTD tests were employed to characterize the effects of bubble aerators layout (i.e. spatial arrangement) on the hydrodynamics in AS reactors. Instead of injecting bubbles through a boundary of the numerical domain, they were generated just above the diffusers via a source term in the continuity equation. This modelling procedure is believed to be more appropriate since it allows setting a 'wall' boundary condition over the membrane diffusers surface.

The results showed that the flow characteristics are extremely sensitive to the aerators layout given the

high gas flow rates used in aerobic AS processes. Among the layouts investigated, the one where diffusers are placed all over the reactor floor generates the flow that best tends toward that of an ideal plug flow reactor. Indeed, this flow field presented the lowest average turbulent diffusion and the most uniform axial velocity and turbulence fields. Such a flow behaviour is expected to be highly beneficial for biological treatment. Indeed, it limits raw wastewater channelling and allows high biological reaction rates as it reduces pollutant dilution by axial diffusion across the reactor. Despite the presence of two recirculation cells, RTD results showed that the global hydrodynamics behaviour of the flow can be conveniently described using the model of continuous-stirred-tank-reactors in series.

The results presented in this paper demonstrate that arranging the membrane aerators in a 'full floor coverage' configuration leads to the least dispersive flow, the highest average gas fraction and the most uniform bubble distribution. Thus, this layout is expected to engender the best treatment efficiency and the largest oxygen transfer rate. However, in order to quantify the benefits provided, a model describing the biochemical reactions and the associated mass transfer equations should be integrated in the CFD model.

Disclosure statement

No potential conflict of interest was reported by the authors.

Funding

This work was supported by the Institut Carnot ICEEL.

References

- [1] Mueller J, Boyle WC, Popel HJ. Aeration: principles and practice. Vol. 11. Boca Raton (FL): CRC Press; 2002.
- [2] Hreiz R, Latifi MA, Roche N. Optimal design and operation of activated sludge processes: state-of-the-art. *Chem Eng J*. 2015;281:900–920.
- [3] Chudoba J, Ottova V, Madera V. Control of activated sludge filamentous bulking—I. Effect of the hydraulic regime or degree of mixing in an aeration tank. *Water Res*. 1973;7(8):1163–1182.
- [4] Rehman U, Vesvikar M, Maere T, et al. Effect of sensor location on controller performance in a wastewater treatment plant. *Water Sci Tech*. 2015;71(5):700–708.
- [5] Fayolle Y, Cockx A, Gillot S, et al. Oxygen transfer prediction in aeration tanks using CFD. *Chem Eng Sci*. 2007;62(24):7163–7171.
- [6] Le Moullec Y, Potier O, Gentric C, et al. Flow field and residence time distribution simulation of a cross-flow gas-liquid wastewater treatment reactor using CFD. *Chem Eng Sci*. 2008;63(9):2436–2449.

- [7] Gresch M, Armbruster M, Braun D, et al. Effects of aeration patterns on the flow field in wastewater aeration tanks. *Water Res.* 2011;45(2):810–818.
- [8] Karpinska AM, Bridgeman J. CFD-aided modelling of activated sludge systems – a critical review. *Water Res.* 2016;88:861–879.
- [9] Laurent J, Samstag RW, Ducoste JM, et al. A protocol for the use of computational fluid dynamics as a supportive tool for wastewater treatment plant modelling. *Water Sci Tech.* 2014;70(10):1575–1584.
- [10] Wicklein E, Batstone DJ, Ducoste J, et al. Good modelling practice in applying computational fluid dynamics for WWTP modelling. *Water Sci Tech.* 2016;73(5):969–982.
- [11] Le Moullec Y, Potier O, Gentric C, et al. Activated sludge pilot plant: comparison between experimental and predicted concentration profiles using three different modelling approaches. *Water Res.* 2011;45(10):3085–3097.
- [12] Alvarado A, Vedantam S, Goethal P, et al. A compartmental model to describe hydraulics in a full-scale waste stabilization pond. *Water Res.* 2012;46(2):521–530.
- [13] Glover GC, Printemps C, Essemiani K, et al. Modelling of wastewater treatment plants – how far shall we go with sophisticated modelling tools? *Water Sci Tech.* 2006;53(3):79–89.
- [14] Potier O, Leclerc JP, Pons MN. Influence of geometrical and operational parameters on the axial dispersion in an aerated channel reactor. *Water Res.* 2005;39(18):4454–4462.
- [15] Fluent. ANSYS fluent theory guide 16.1. Canonsburg (PA): ANSYS Inc; 2015.
- [16] Sokolichin A, Eigenberger G, Lapin A. Simulation of buoyancy driven bubbly flow: established simplifications and open questions. *AIChE J.* 2004;50(1):24–45.
- [17] Clift R, Grace JR, Weber ME. Bubbles, drops, and particles. New York (NY): Academic Press; 1978.
- [18] Moraga FJ, Bonetto RT, Lahey RT. Lateral forces on spheres in turbulent uniform shear flow. *Int J Multiph Flow.* 1999;25:1321–1372.
- [19] Troshko AA, Hassan YA. A two-equation turbulence model of turbulent bubbly flow. *Int J Multiph Flow.* 2001;27(11):1965–2000.
- [20] Gualtieri C, Angeloudis A, Bombardelli F, et al. On the values for the turbulent schmidt number in environmental flows. *Fluids.* 2017;2(2):17–44.
- [21] Vial C, Poncin S, Wild G, et al. A simple method for regime identification and flow characterisation in bubble columns and airlift reactors. *Chem Eng Process: Process Intensif.* 2001;40(2):135–151.
- [22] Juliá JE, Hernández L, Chiva S, et al. Hydrodynamic characterization of a needle sparger rectangular bubble column: homogeneous flow, static bubble plume and oscillating bubble plume. *Chem Eng Sci.* 2007;62(22):6361–6377.